7-5-2016

# Effects on the pore structure and permeability change by coke deposition during crude oil in-situ combustion

Qianghui Xu
*Tsinghua University*, xuqh12@mails.tsinghua.edu.cn

Bin Ma
*Tsinghua University*

Hang Jiang
*China National Petroleum Corporation*

Ran Xu
*Tsinghua University*

Chao Huang
*Tsinghua University*

***See next page for additional authors***

**Authors**
Qianghui Xu, Bin Ma, Hang Jiang, Ran Xu, Chao Huang, and Lin Shi

**Proceedings of the 6th International Conference on Porous Media and Its Applications in Science and Engineering**
**ICPM6**
**July 3-8, 2016, Waikoloa, Hawaii**

# EFFECTS ON THE PORE STRUCTURE AND PERMEABILITY CHANGE BY COKE DEPOSITION DURING CRUDE OIL IN-SITU COMBUSTION

**Qianghui Xu**, **Bin Ma**, **Ran Xu**, **Chao Huang**, **Lin Shi**
*Key Laboratory for Thermal Science and Power Engineering of Ministry of Education, Department of Thermal Engineering, Tsinghua University, Beijing, 100084, China*
*Email: xuqh12@mails.tsinghua.edu.cn*

**Wei Long**
*iCore Digital Reservoir Group, Katy, Texas, 77450, United States*

**Hang Jiang**
*State Key Laboratory of Enhanced Oil Recovery, Research Institute of Petroleum Exploration & Development, China National Petroleum Corporation, Beijing, 100007, China*

## ABSTRCT

In-situ combustion (ISC) is an important thermal recovery technique. Significant open ISC questions include the effect of coke formation on the pore structure and permeability. In the study, the combination of X-ray computed microtomography (*u*CT) and LB simulation was used to evaluate the evolution of the geometric properties and the permeability with coke deposition. The geometric properties with different coke depositions were extracted by image analysis, such as porosity, geometric tortuosity and pore throat size distribution. The permeabilities of the microstructures were computed by LB simulation. The results showed that permeabilities of the microstructures with coke deposition were overestimated averagely by 40.6% by Kozeny-Carman correlation. The overestimation is due to that the coke deposition complicated the microstructures and then arose more fluid stagnant flow with the fluid path tortuosity increasing. According to the workflow, the permeability change with coke deposition during ISC is highly expected to be characterized accurately at the Darcy scale.

## INTRODUCTION

In-situ combustion (ISC) is an enhanced oil recovery technique to exploit the unconventional crude oil resources with high recovery efficiency (Mahinpey et al. 2007). Great amount of reaction heat is released in-place by burning the solid residue, so-called coke at the combustion front with the heated temperature higher than 400℃. As the mature of horizontal well technology, the integration of horizontal well and in situ combustion process has been proposed such as Toe—Heel Air Injection (THAI).

The solid coke residue on the sand grain surface is the main fuel consumed in the oil reservoir. However, the coke deposited in the porous medium reduce the porosity and permeability (Xu et al. 2016). The effect of coke deposition on the oxygen transport further promotes the oxygen bypassing in the reservoir, especially at the combustion front. The bypassing oxygen then impacts the air participating in the crude oil low temperature oxidation in the evaporation and vis-breaking zones (Dabbous and Fulton 1974) and

then the combustion front spreading characteristics. In the THAI process, the coke deposition inside the production well creates a gas seal that prevents air breakthrough into the producer and stabilizes the THAI process(Xia et al. 2005). The STARS simulator by Computer Modelling Group Ltd. provides a function to specify the variable permeability affected by coke deposition. However, the parameters still need to be supported by reliable data guided by the tutorial. Unfortunately, little study is available about the effects of permeability changes on the amounts of coke deposition in ISC or THAI processes. Xu et al. presented an experimental study to physically simulate coke formation during crude oil ISC process with in-situ measurement of the post-deposition permeability (Xu, et al. 2016). The heterogeneous coke concentration distribution in the 20 cm long cores led to the inaccurate prediction of the global permeability only in terms of the average coke concentration of the whole core (Xu, et al. 2016). The permeability change during coke deposition for ISC or THAI processes need to be characterized more accurately to reduce the simulation uncertainties.

X-ray computed microtomography ($\mu$CT) has been used to efficiently quantify the relationship between the material microstructure and their transport properties, especially in the geoscience and geo-environmental fields (Liu et al. 2014; Moreno-Atanasio et al. 2010). Quantification of geometric and transport properties related to the coked cores based on real microstructures are rare. Applying the non-destructive $\mu$CT to the coked cores can resulted in 3D microstructure reconstructions mapped by X-ray attenuation coefficients (Leu et al. 2014). Gray-scale intensities of the X-ray attenuation coefficients varies from the materials due to material properties such as density and atomic number (Moreno-Atanasio et al. 2010). Depending on the significant gray-scale intensity contrast, image segmentation can assign the image regions with different gray levels as different materials. However, the questionable problem of the present study is whether the pore (air), coke and glass beads can be distinguished by their gray-scale intensity contrasts. Meanwhile, the uncertain input parameters for the segmentation algorithms determines the gray-scale thresholds of the different materials, then resulting in an artificial errors of the material volume fractions and the microstructure geometric and transport properties. Therefore, more experimental data is needed to support the image processing.

The porosity, geometric tortuosity and the pore throat size distribution are considered as important geometric parameters (Keller et al. 2015; Liu et al. 2016). Knowing the geometric properties affected by the coke deposition helps understand the transport property characteristics. The previous SEM study showed that a portion of the coke was coated on the glass bead surfaces with the rest in pore bridges and in pores (Xu et al. 2016) . The coke consolidated the glass bead matrix and complicated the pore structure. How the coke deposition impacts the geometric and transport properties is still unclear. Recently, the Lattice Boltzmann (LB) pore-scale simulation has been used to visualize the fluid flow and compute the permeability and diffusivity of digital cores (Chen et al. 2009). The image resolution significantly influenced the prediction accuracy of the permeability (Arns et al. 2004), especially for the coked cores where the thickness of the coating coke film on the glass bead surfaces is only 1-2 um. Therefore, the high resolution $u$CT should be used in the study. However, the high resolution in turn reduces the sample size for $u$CT. For the representative permeability prediction, therefore, the representative volume element (RVE) of the digital coked cores should be assessed in advance. Meanwhile，Liu et al showed the computing cost is as high as the order of a few days by using 96 cores by LB simulation for the digital cores of about $500^3$ size (Liu et al. 2016). The LB programs need to be further optimized.

In the study, coked glass bead clusters with different amount of coke deposition were sampled. The coke volume fractions and the porosity are experimentally measured, which were used as important criterions for the image segmentation. The coked glass bead

microstructures were reconstructed by *u*CT with 1um spatial resolution and were characterized with the coke, glass beads and pores distinguished by image processing. The digital microstructure geometric properties with different coke deposition were then extracted by image analysis, such as porosity, geometric tortuosity and pore throat size distribution. The method of Keller et al. was used to estimate the the porosity RVE size (Keller et al. 2013). Then, the permeabilities of the microstructures with different coke deposition were computed by the LB simulation by an in-house developed program. The permeability damage predicted by the workflow was compared with the prediction by Kozeny-Carman (K-C) correlation to evaluate the evolution of the permeability with the coke deposition.

# 1. Methodology

## 1.1 Sampling

A crude oil from the Xinjiang Reservoir was selected for this study. 250-325 mesh glass beads were used for the porous medium in order to better quantify the effect of coke deposition on geometric properties and permeability change than the sandstones in irregular shape and size. An experimental apparatus (Xu et al. 2016) subjected the oil saturated core samples to a programmed experimental environment similar to rocks in reservoirs undergoing in-situ combustion with a pressure of 5.0 MPa, then produced the coked cores. Six coked glass bead clusters were sampled with the coke mass fraction at 3.99~5.92%. They were then cut carefully to 1 $mm^3$ size to acquire the *u*CT images.

The coke mass fractions were measured by the thermogravimetry analysis (TGA). The average density of the coke was 1.11 $g/cm^3$ and the density of the glass density was 2.49 $g/cm^3$ both measured by true density meter. The coke volume fractions were then calculated based on the coke mass fractions and the coke and glass bead densities. Since the individual sampled coked glass bead cluster almost weighed less than 100 mg, the porosity experimental error of the single coked glass bead cluster was significant. Therefore, a series of the coked glass bead clusters were selected for the porosity measurement, of which the individual coke mass fraction concentrated in 5.30%~6.00% range and averaged 5.66%.

## 1.2 Tomographic imaging and image processing

A *u*CT unit produced by Sanying Precision Instruments Ltd, with a 40-keV X-ray source was used to scan the samples with a 1 um spatial resolution. The low X-ray beam intensity achieved the significant gray-scale intensity contrasts. The gray-scale intensity differences of the coke、pore and glass beads can be viewed in Figure 1a, which shows the voxels of the glass beads appear brighter and the voxels of pore appear darker, while the voxels of the coke trapped in the pores exhibit gray.

The 16-bit image contrast was enhanced by histogram equalization. Median filter was applied to the *u*CT gray-scale images to remove the salt and pepper noise, especially in the glass bead regions. The image after noise filter is shown in Figure 1b for comparison. The holes inside the glass beads as the dead-end void space were then filled by several processing procedures, which included most of those open holes as shown in Figure 1c. The glass beads were then separated by a marker-based watershed algorithm based on the maps of the geometrical distance between the glass bead pixels and the others. The marker-based watershed algorithm marked the innermost regions (region maximal) inside the glass beads as the seeds. The computed separation lines worked well to isolate the glass beads, as showed in Figure 2a. The isolated glass beads benefited the statistics of the equivalent diameter and the sphericity, but also removed the excessive false contacts between the adjacent glass beads, which blocked fluid flow paths.

In order to overcome the noise and partial volume effects blurring the phase transitions, the robust watershed segmentation algorithm was applied to partition the images into the pore, coke and the glass bead phases. During the algorithm, safe regions corresponding to different phase interior was firstly selected as the seeds and they expanded to the actual phase boundaries later based on the gray-scale

gradient maps. The experimental data about the porosity and the coke volume fractions help select the seed gray level thresholds. The resulting 2D image slice is showed in Figure 2b. The blue is the glass beads, the black is the pores and the colorful regions are the coke. Examples of 3D digital glass bead matrix and the digital coked glass beads matrix are also illustrated in Figure 3a and Figure 3b.

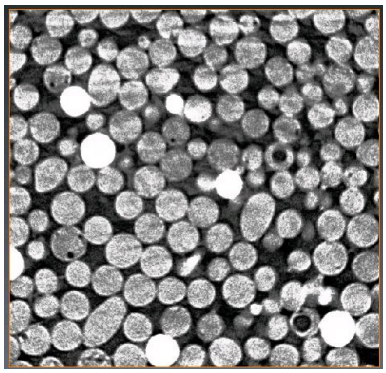

a) Gray-scale image slice before noise filter

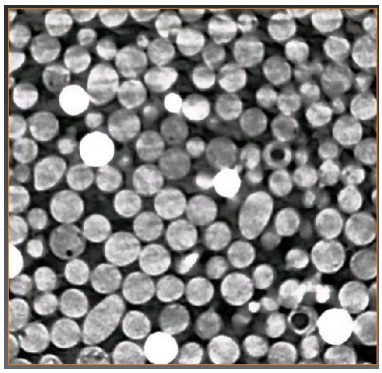

b) Gray-scale image slice after noise filter

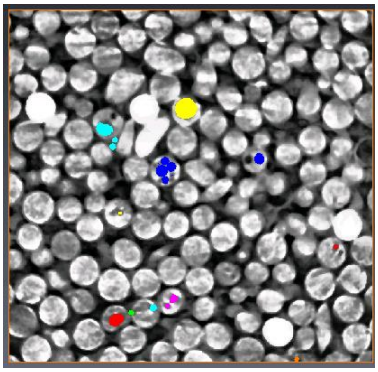

c) Fill holes

Figure 1. Images that show the image processing steps about noise filter and hole filling

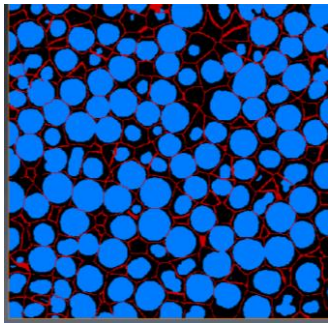

a) Separation lines to isolate glass beads

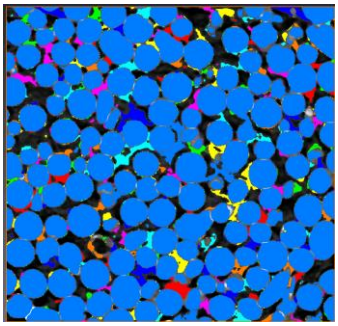

b) 2D image slice after watershed segmentation

Figure 2. Images that show the image processing steps about glass bead separation and image segmentation

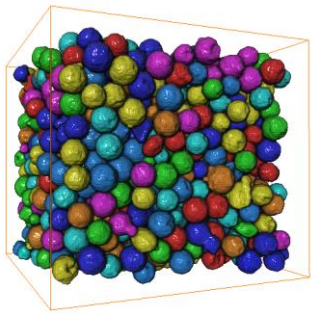

a) 3D digital Glass bead matrix

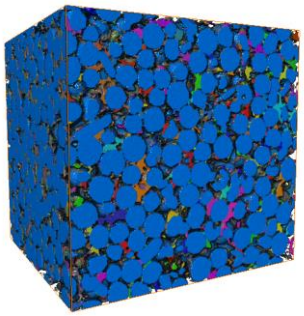

b) 3D digital coked glass bead matrix

Figure 3. Reconstructed microstructures based on *u*CT and image processing techniques

The porosity RVE size was estimated based on the method of Keller et al. (Keller et al. 2013).Geometric

parameters such as porosity, geometric tortuosity and pore throat size distribution were all extracted from the 3D digital microstructures. The geometric tortuosity was calculated based on the Gommes et al. approach (Gommes et al. 2009; Keller et al. 2015).

### 1.3 LB simulation and permeability predictions

The 3D digital microstructures were directly used to define the internal boundary for the pore-scale fluid flow in LB simulation. The D3Q15 LB model (3 dimensions and 15 velocity directions) was employed in the study. The LB code was in-house developed. All the six external boundaries of the 3D processed images were defined as periodicity boundary conditions, while the source force was added in the z direction as the driving force of the fluid flow. According to the Darcy law, The permeabilities of the microstructure were calculated based on the source force and the mass flow in the z direction.

## 2. Results and Discussion

### 2.1 image segmentation validations

The coke actually contained non-ignorable microscale pores inside observed by SEM images in the previous study, however, the *u*CT resolution used was larger than the micropore size. As a result, the coke internal micropore could not be characterized and then all treated as the coke phase during the reconstruction and image processing. Since the internal porosity of the coke was difficultly measured, 15% porosity of the coke was assumed based on the porosities of other disorder carbonaceous materials. During the watershed segmentation, therefore, the input thresholds of the phase seeds were modified to take in the extra “coke volume” instead of the indistinguishable coke microspore, based on the experimental coke volume fractions. Therefore, the image-analysis-based coke volume fractions were averagely 1.41% higher than the experimental results as shown in Figure 4a. Meanwhile, the porosity of the coked glass bead cluster samples was 29.9% measured by mercury porosimeters, whose coke mass fraction averaged 5.66%. The average imaged-analysis-based porosity of two digital coked glass bead matrix was 29.8%, whose coke mass fraction averaged 5.52%. The image-based-analysis and experimental porosities were consistent, indicating the reasonable image segmentation. The statistics of the glass beads showed the equivalent diameter distribution more highly concentrated compared to the normal distribution with an average of 46.8 *u*m as shown in Figure 4b, and the median sphericities of the glass beads approached one. The result showed the image segmentation also worked well to keep the features of the glass beads.

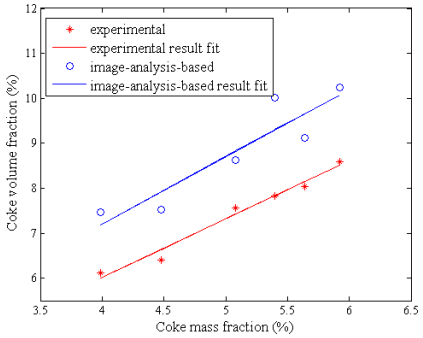


a) Variations of experimental and image-analysis-based coke volume fraction with coke mass fraction

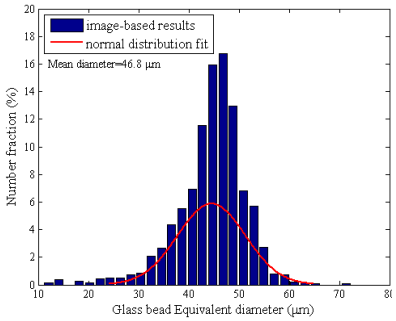


b) Equivalent diameter distribution of Glass beads

Figure 4. Statistic of the coke volume fraction and the glass bead diameter

### 2.2 RVE studies

The local porosity distributions were obtained from the reconstructed microstructures with and without the coke deposition, following the method of Keller et al. (Keller et al. 2013). An example of the local porosity distribution is showed in Figure 5a and Figure 5c. With the increase in the subdomain size *L*, the local porosity distribution curves changed toward a narrow distribution with increasing remarkable single peak, especially for the subdomain size of 480 pixels. Meanwhile, Figure 5b and Figure 5d also showed that

the porosity standard deviation decreased but the mean porosity floated little as a function of the subdomain size. When the subdomain size was $480^3$ pixels, the coefficient of variance (COV) of the porosity was 0.81% for the pure glass bead matrix and 0.36% for the coked glass bead matrix, which were both significantly lower than the COV criterion of 20% (Chen et al. 2013). Therefore, the glass bead matrix with and without coke deposition both homogeneous at the scale of 480 *u*m and the scale was then taken as the RVE size. The geometric and transport properties were analyzed at the RVE as follows.

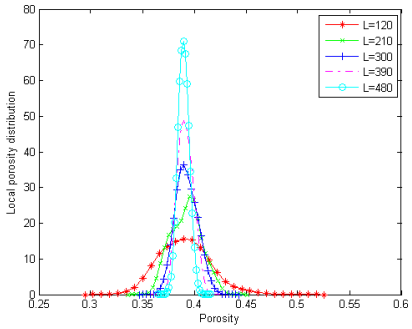


a) Local porosity distribution of pure glass bead matrix with the subdomain size

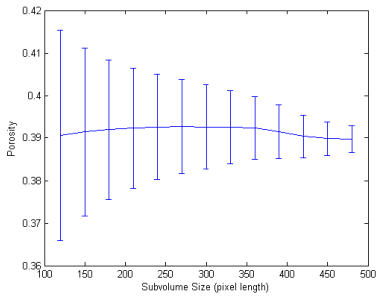


b) Glass bead matrix: image-analysis-based porosity with the subdomain size

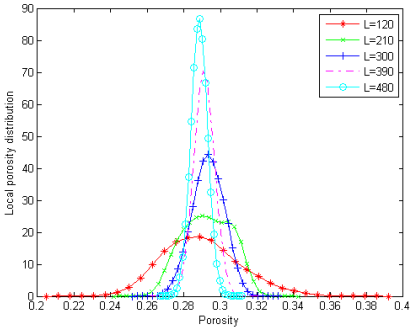


c) Local porosity distribution of the coked glass bead matrix with the subdomain size

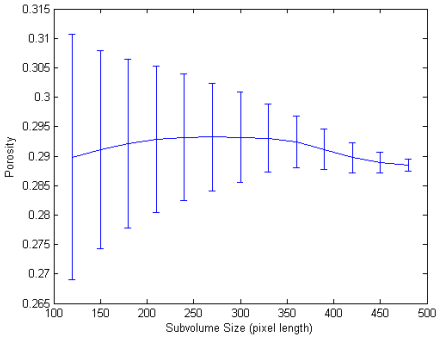


d) Coked glass bead matrix: image-analysis-based porosity with the subdomain size

Figure 5. REV studies for the microstructures with and without coke deposition

### 2.3 Pore throat distribution

Figure 6a shows the percentages of the pore throats in difference size ranges changed with coke deposition. The pore throats at 1-5 um range increased much with the coke deposition, while the pore throats larger than 15 um decreased significantly. As the amount of coke deposition increased, the percentage increments of pore throats at 1-5um kept increasing, as shown in Figure 6b. Therefore, the result indicated the pore throat distribution shifted toward to the size at 1-5 um with the pores at 1-5 um as the primary due to the coke deposition.

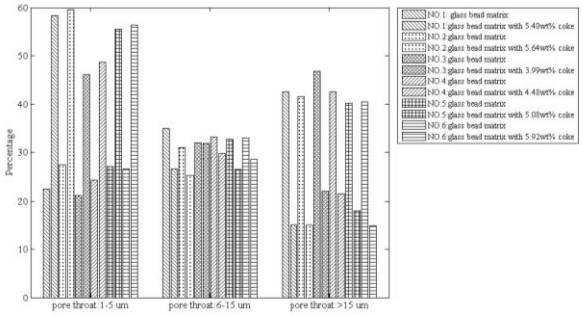


a) Variations of the percentages of the pore throats in different size ranges with coke deposition: 1-5um; 6-15 um; > 15 um

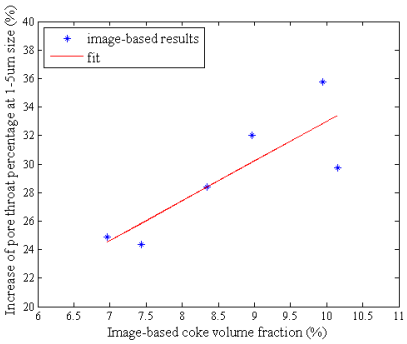


b) Variations of the percentage increments of pore throat at 1-5 um size with the coke volume fractions

Figure 6. Changes of the pore throat distribution with the coke deposition

## 2.4 Geometric tortuosity

The geometric tortuosity along the z direction was calculated following the method of Gommes et al. (Gommes et al. 2009; Keller et al. 2015). The geodesic distance represents the shortest path between the pore voxels. The connecting line entirely lies within the pore space, not through the solid matrix. The geometric tortuosity between the two voxels is then defined as the ratio of the geodesic distance and the Euclidian distance, the latter of which represents the parallel plane distance. The geodesic distances between the source xy-plane at z=0 and all the other pore voxels along the z direction were firstly mapped by a chessboard distance algorithm implemented in Avizo software, as shown in Figure 7a. By analyzing all image planes, the tortuosity of a reconstructed microstructure was then calculated as the slope of linear fit of the average geodesic distances within each plane and the corresponding Euclidian distances. Figure 7b indicated the tortuosity increased as the porosity decreased due to the coke deposition. However, the quantification showed that the geometric tortuosity did not increase significantly, only by 2.85% as the amount of the coke deposition was 5.92%. Compared to the coke deposition ranging from 3.99%~5.92%, the original high porosity of the glass bead matrix (35%~40%) was suggested to result in the non-significant increase in the tortuosity. Even through some large pores were blocked as indicated by the pore throat distribution analysis, the connectivity along the pore space was not greatly affected.

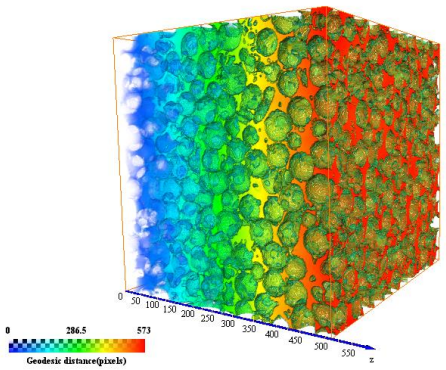


a) Geodesic distance from the limit z=0 to any pore voxel for the glass bead matrix with coke deposition

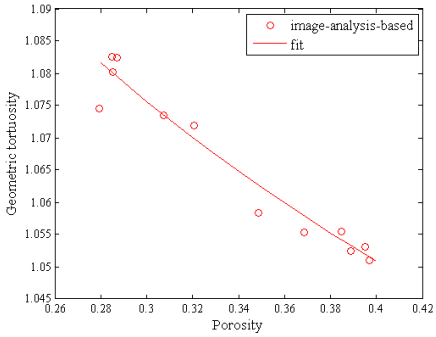


b) Variance of geometric tortuosity with the porosity

Figure 7. Methods to calculate the geometric tortuosity and the result

## 2.5 simulation of fluid flow and permeability prediction

The pore-scale fluid flow was simulated by LB method. To validate the in-house developed programs, the Poiseuille flow was simulated in a 3D circular tube. Figure 8a shows that the numerical dimensionless radial velocity distribution is consistent with the analytical solution. The permeabilities of the digital glass bead matrix were predicted by the LB simulation. The result agreed with the predictions by the K-C correlation, as shown in Figure 8b. The average absolute difference between the numerical and empirical solution was only 4.54%. For the RVE size of $480^3$ voxel, the LB computational cost for the pure glass bead matrix was about 0.5 h while the computational cost increased to about 3.0 h for the

coked glass bead matrix due to the complicated fluid field, when using 120 CPU processors. The latter computational cost was still highly acceptable compared to the previous studies (Liu et al. 2014).

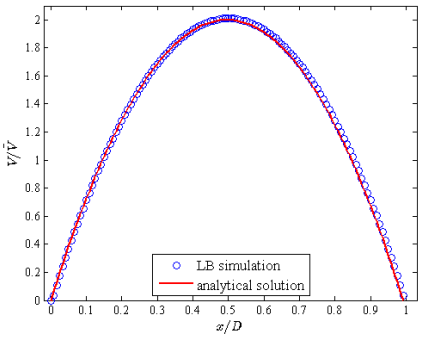


a) Analytical solution and LB numerical results for non-dimensional radial velocity distribution during the Poiseuille flow.

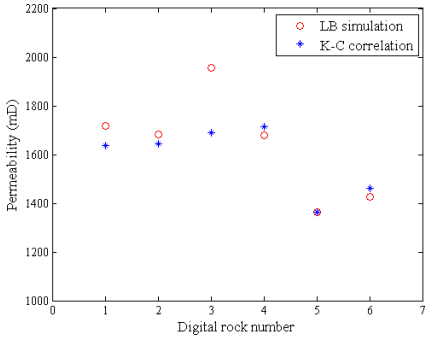


b) Permeability of Digital Glass Bead Matrix predicted by LB simulation and K-C correlation

Figure 8. Validation of the in-house developed LB code

Figure 9 visualizes the pore scale gas flow through the microstructures with and without the coke deposition. By the visual observation, the fluid flow paths seem more tortuous inside the coked glass bead matrix than those inside the pure glass bead matrix, which was consistent with the geometric tortuosity analysis. Meanwhile, the probability density functions (pdf) of the longitudinal velocity along the z direction are plotted in Figure 10. Coke deposition concentrated the velocity distribution with the peak near zero and then reduced the mean longitudinal velocity. The increasing peak near zero also showed that the stagnant flow increased with coke deposition due to more impassable solid matrix, resulting in the increase in the dead-end pores and then more tortuous pore-scale fluid paths.

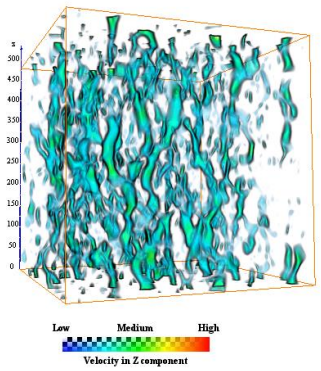


a) 3D flow filed along z direction inside the pure glass bead matrix

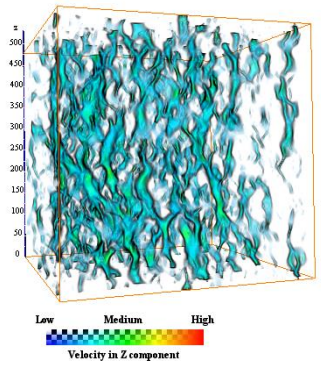


b) 3D flow filed along z direction inside the coked glass bead matrix

Figure 9. Visulization of the pore-scale fluid flow

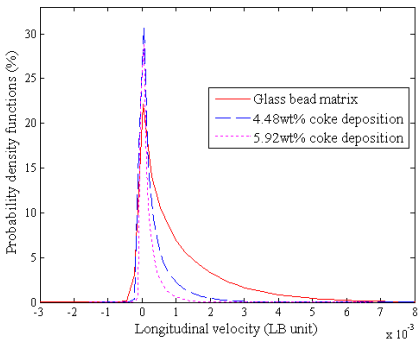


Figure 10. Probability density functions of longitudinal fluid velocity

Permeabilities of the microstructures with different amount of coke deposition were computed by the LB method，as shown in Figure 11a. By comparison to the predictions by K-C correlation, the numerical were averagely 40.6% lower than the empirical solutions.

The differences were more significant than those for the pure glass bead matrix. Therefore, the results showed the permeabilities of the microstructures with the pure glass bead matrix could be accurately predicted by the K-C correlation, however, the permeabilities of the microstructures with coke deposition were overestimated by K-C correlation. The normalized reduced permeabilities (Xu et al. 2016) were in turn underestimated by about 20% by the K-C correlation compared to the numerical results, as shown in Figure 11b. As the geometric properties and flow fields analyses, the coke deposition increased the microstructure complication and then arose more fluid stagnant flow with the tortuosity of the fluid path increasing. The analyses were suggested to result in the prediction deviation by K-C correlation. The present study also showed that the normalized reduced permeabilities could not be modelled by a format like the K-C correlation but with the power exponent of the porosity modified, as the function given by commercial STARS simulator. Figure 11b indicated the normalized reduced permeabilities almost increased linearly with the amount of coke deposition at 3.99%~5.92% mass fraction range.

Correlating the normalized reduced permeability with the porosity and the tortuosity needs more data according to the workflow, which will be implemented in the future. According to the workflow, the permeability change with the coke deposition for ISC can be characterized more accurately at the Darcy scale compared with the experimental tests due to the heterogeneous coke deposition in the experimental core tubes.

## CONCLUSIONS

The combination of *u*CT and LB simulation was used to evaluate the evolution of the permeability and the geometric properties with the coke deposition during ISC. A 1 um spatial resolution of *u*CT images were obtained and the coked glass bead microstructures were then characterized. The image segmentation was experimentally validated. The subdomain size of $480^3$ voxels was taken as the porosity REV scale. With the coke deposition increasing to 5.92%, the pore throat distribution shifted toward to the size at 1-5 um with the pores at 1-5 um as the primary. However, the geometric tortuosity did not increase significantly only by 2.85%. The permeabilities of the microstructures with pure glass bead matrix could be accurately predicted by the K-C correlation, however, the permeabilities of the microstructures with the coke deposition were overestimated averagely by 40.6% by the K-C correlation. The overestimation is due to that the coke deposition complicated the microstructures and then arose more fluid stagnant flow with more tortuous fluid paths. The study suggested the normalized reduced permeability could not be modelled only by a format like the K-C correlation but modifying the power exponent of the porosity. According to the workflow, the permeability change during coke deposition for ISC is highly expected to be characterized accurately at the Darcy scale.

## ACKNOWLEGEMENTS

The work was supported by the State Key Program of the National Natural Science Foundation of China (Grant No: 512366004) and the Science Fund for Creative Research Groups (No. 51321002). The work was also supported by the National Science and Technology Major Project (2011ZX05012) and the PetroChina Technology R&D Project on the New Technology and Method for Oil & Gas Development (2014A–1006).

## REFERENCES

[1] Arns CH, Knackstedt MA, Pinczewski WV, Martys NS (2004) Virtual permeametry on microtomographic images. Journal of Petroleum Science and Engineering. 45(1):41-46.

[2] Chen C, Hu D, Westacott D, Loveless D (2013) Nanometer‐scale characterization of microscopic pores in shale kerogen by image analysis and pore‐scale modeling. Geochemistry, Geophysics, Geosystems. 14(10):4066-4075.

[3] Chen C, Lau BL, Gaillard JF, Packman AI (2009) Temporal evolution of pore geometry, fluid flow, and solute transport resulting from colloid deposition. Water resources research. 45(6): W06416,

doi:10.1029/2008WR007252
[4] Dabbous MK, Fulton PF (1974) Low-Temperature-Oxidation Reaction Kinetics and Effects on the In-Situ Combustion Process. Society of Petroleum Engineers Journal. 14(03):253 - 262.
[5] Gommes CJ, Bons AJ, Blacher S, Dunsmuir JH, Tsou AH (2009) Practical methods for measuring the tortuosity of porous materials from binary or gray‐tone tomographic reconstructions. AIChE Journal. 55(8):2000-2012.
[6]Keller LM, Holzer L, Schuetz P, Gasser P (2013) Pore space relevant for gas permeability in Opalinus clay: Statistical analysis of homogeneity, percolation, and representative volume element. Journal of Geophysical Research: Solid Earth. 118(6):2799-2812.
[7] Keller LM, Hilger A, Manke I (2015) Impact of sand content on solute diffusion in Opalinus Clay. Applied Clay Science. 112:134-142.
[8] Leu L, Berg S, Enzmann F, Armstrong RT, Kersten M (2014) Fast X-ray Micro-Tomography of Multiphase Flow in Berea Sandstone: A Sensitivity Study on Image Processing. Transport in Porous Media. 105(2):451-469.
[9] Liu J, Pereira GG, Regenauer-Lieb K (2014) From characterisation of pore-structures to simulations of pore-scale fluid flow and the upscaling of permeability using microtomography: A case study of heterogeneous carbonates. Journal of Geochemical Exploration. 144:84-96.
[10] Liu J, Pereira GG, Liu Q, Regenauer-Lieb K (2016) Computational challenges in the analyses of petrophysics using microtomography and upscaling: A review. Computers & Geosciences. 89:107-117.
[11] Mahinpey N, Ambalae A, Asghari K (2007) In Situ Combustion in enhanced oil recovery (EOR): a review. Chemical Engineering Communications. 194(8):995-1021.
[12] Moreno-Atanasio R, Williams RA, Jia X (2010) Combining X-ray microtomography with computer simulation for analysis of granular and porous materials. Particuology. 8(2):81-99.
[13] Xia T, Greaves M, Turta A (2005) Main Mechanism for Stability of THAI-Toe-to-Heel Air Injection. Journal of Canadian Petroleum Technology. 44(01): 42-48.
[14] Xu QH, Jiang H, Zan C, Tang W, Xu R, Huang J, Li Y, Ma D, Shi L (2016) Coke Formation and Coupled Effects on Pore Structure and Permeability Change During Crude Oil In-situ Combustion. Energy & Fuels. 30: 933-942.